Deconvolution of femtosecond time-resolved spectroscopy data in multivariate curve resolution. Application to the characterization of ultrafast photo-induced intramolecular proton…

ARTICLE *in* JOURNAL OF CHEMOMETRICS · JULY 2010

Impact Factor: 1.5 · DOI: 10.1002/cem.1315

Special Issue Article

Journal of CHEMOMETRICS

Received: 30 July 2009, Revised: 5 January 2010, Accepted: 1 March 2010, Published online in Wiley InterScience: 15 April 2010

(www.interscience.wiley.com) DOI: 10.1002/cem.1315

Deconvolution of femtosecond time-resolved spectroscopy data in multivariate curve resolution. Application to the characterization of ultrafast photo-induced intramolecular proton transfer

Nicolas Mouton[a], Michel Sliwa[a], Guy Buntinx[a] and Cyril Ruckebusch[a]*

In femtosecond absorption spectroscopy, deconvolution of the measured kinetic traces is still an important issue as photochemical processes that may possess shorter characteristic times than the time resolution of the experiment are usually considered. In this work, we propose to perform deconvolution of the time-dependent concentration profiles extracted from multivariate curve resolution (MCR) applied to spectrokinetic data. The profiles are fitted with a model function including a description of the instrumental response function (IRF) of the experiment. The method combines the potential benefits of soft-modeling data analysis with the ones of hard-modeling for parameter estimation. The potential of the method is demonstrated first analyzing five synthetic data sets for which IRF of different widths are simulated. It is then successfully applied to resolve femtosecond UV-visible transient absorption spectroscopy data investigating the photodynamics of salicylidene aniline, a photochromic molecule of wide interest. Considering a time resolution of 150 fs for the IRF, a characteristic time of 45 fs is recovered for the first step of the photo-induced process which consists of an ultrafast intramolecular proton transfer. Our results also confirm the existence of an intermediate species with a characteristic time of 240 fs. Copyright © 2010 John Wiley & Sons, Ltd.

Keywords: MCR-ALS; kinetic profiles; deconvolution; transient absorption spectroscopy; proton transfer

1. INTRODUCTION

Transient absorption spectroscopy is a powerful technique widely used to investigate photo-induced chemical processes ranging from femtoseconds to milliseconds time scale [1–4]. For ultrafast processes of characteristic time in the sub-picosecond time domain, any electronic apparatus can follow signal variations and transient absorption spectroscopy is thus based on the use of two short laser pulses (~100 fs). The former is a monochromatic pulse (pump) that triggers the reaction. The latter is a white light spectrum (probe) that enables to record a transient spectrum using a multichannel spectrometer. To follow the evolution of transient species, the delay between the pump and the probe is controlled by gradually varying an optical delay line (a 3 μm pathlength difference corresponds approximately to a delay time step of 1 fs). Nevertheless, the time resolution of transient absorption experiments is usually on the order of a few hundreds of femtoseconds due to pulse overlapping and broadening [5]. Additionally, nonlinear optical effects may also distort the measured signals [5,6]. This latter issue can be dealt with by analyzing multi-experiment data with multivariate curve resolution (MCR), as recently reported [7]. In the current work, we first bring our attention to the characterization of the time resolution assessing the instrumental response function (IRF) from the measurement of pump–probe cross-correlation signal [6,8]. We then use this measurement to perform deconvolution and to recover pure kinetics by fitting the time-dependent concentration profiles extracted from MCR.

Recording transient absorption values as a function of time and wavelength provides two-way data (the so-called spectrokinetic data). To characterize the mechanism of the photo-induced process studied requires then resolving spectrokinetic data into pure components: time-dependent concentration profiles and corresponding transient absorption spectra. For this purpose, the potential of soft-modeling methods in ultrafast time-resolved spectroscopy has been recently pointed out [9–12]. To perform component resolution of unknown reactions, soft-modeling MCR methods [13,14] may provide powerful alternative to parametric methods more conventionally applied in the field of femto-chemistry [15]. Furthermore, MCR methods can be extended to include refinement of the time-dependent concentration profiles (more generally any profiles) fitting them with a kinetic model (hard-model) to assess reaction constants and increase the

* *Correspondence to: C. Ruckebusch, Laboratoire de Spectrochimie Infrarouge et Raman, LASIR CNRS UMR 8516, Université de Lille 1, bât C5, 59655 Villeneuve d'Ascq, France.*
E-mail: cyril.ruckebusch@univ-lille1.fr

a *N. Mouton, M. Sliwa, G. Buntinx, C. Ruckebusch*
Laboratoire de Spectrochimie Infrarouge et Raman, LASIR CNRS UMR 8516, Université de Lille 1, bât C5, 59655 Villeneuve d'Ascq, France

robustness of the resolution [16,17]. The potential of this kind of approach mixing hard- and soft-modeling has been shown in time-resolved spectroscopy [7,9,10,18].

As time resolution is usually a few hundreds of femtoseconds, any transient phenomena occurring faster, or on the same timescale, are affected by the convolution of the true kinetics with the IRF. Direct deconvolution of the kinetic traces can be performed by fitting the model function [6], by model-free methods using inverse filtering based on Fourier transformations [19–21] or by methods based on genetic algorithms [22]. We propose here to tackle the problem of deconvolution in the frame of MCR by fitting the time-dependent concentration profiles extracted from the MCR resolution into pure components with a function including the description of the IRF. The advantages of this approach are manifolds. First, the resolution and deconvolution of the profiles do not require explicit knowledge of a kinetic model. Second, the IRF parameter may be fixed using values estimated from measurement (no additional parameters to be fitted). The main advantage when compared to more conventional global analysis is that the external fitting procedure is performed on the concentration profiles resolved from soft-modeling. Components that do not contribute to the signal in the spectral domain may thus be included in the fit. On the other hand, profiles corresponding to identified non-kinetic species may be kept outside the fitting procedure. Additionally, this approach may be less sensitive to experimental noise than applying a more classical deconvolution method. It should be added that this work is the first step towards the more general implementation of adequate models for the resolution of convoluted spectrokinetic data into hybrid hard- and soft-modeling MCR procedures.

The proposed strategy is applied to the study of the photochromism of anils by femtosecond UV-visible transient absorption spectroscopy. Photochromism is a reversible photochemical reaction between two forms having different absorption spectra [23,24]. Photochromic materials are still being intensively studied for their potential application in optical devices, from ophthalmic lenses to optical memories and ultra-fast switches [25,26]. In this respect, we are currently focusing on anils such as salicylideneaniline (SA) and its derivatives [27,28]. The photo-reaction is based on an excited-state intramolecular proton transfer (ESIPT) between an enol and a keto form of the molecule (Figure 1), which then creates the photoproduct. The detailed mechanism is still controversial but the ESIPT usually occurs in less than 50 fs in solution [29–34]. In the previous analysis [7], new insights into the photo-reaction were obtained but as deconvolution was not considered, the kinetic analysis had to be considered very carefully at ultrashort time scale.

The paper is organized as follows: Section 2 describes the materials and methods introducing femtosecond pump–probe spectroscopy and measurement of the IRF. Section 3 gives an overview of MCR methods and details the procedure implemented for deconvolution of the resolved kinetic profiles. Section 4 presents the different data sets used in this study. Section 5 contains results and discussion for simulated data, with characteristic times below, equal and superior to the IRF; and for femtosecond transient absorption spectroscopy data.

2. FEMTOSECOND TRANSIENT ABSORPTION SPECTROSCOPY

The femtosecond transient absorption set-up has been described elsewhere [35,36]. Briefly, in our experiments, a 1-kHz Ti:sapphire laser system (Coherent oscillators and a BM Industries regenerative amplifier) delivers 80 fs (0.8 mJ) pulses at 780 nm. The pump pulse is set at 390 nm by frequency doubling the fundamental beam. The pump pulse energy at the sample is 6 μJ with a pump diameter of about 0.5 mm (3 mJ/cm^2). The white light continuum probe beam is generated by focusing the fundamental beam in a 1 mm CaF_2 rotating plate. The pump–probe polarization configuration is set at the magic angle (54.7°) and the probe pulse is delayed in time relative to the pump pulse using an optical delay line (Microcontrol Model, precision (0.1 μm)). The white light continuum is split into a probe

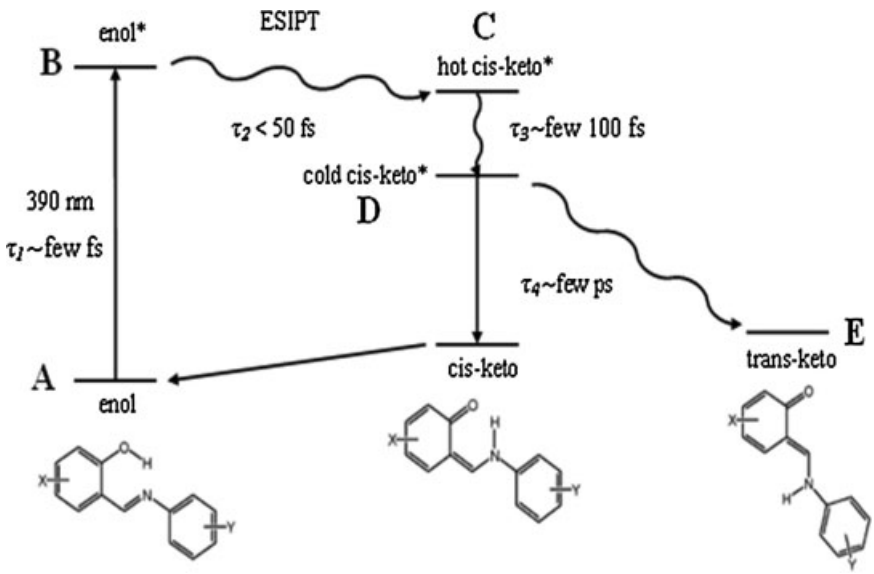

Figure 1. Overall photo-induced process for anils. Each species and time constant are named and numbered (*A*, *B*, *C*, *D*, *E* and 1, 2, 3, 4) with regards to the MCR data analysis (see Section 5).

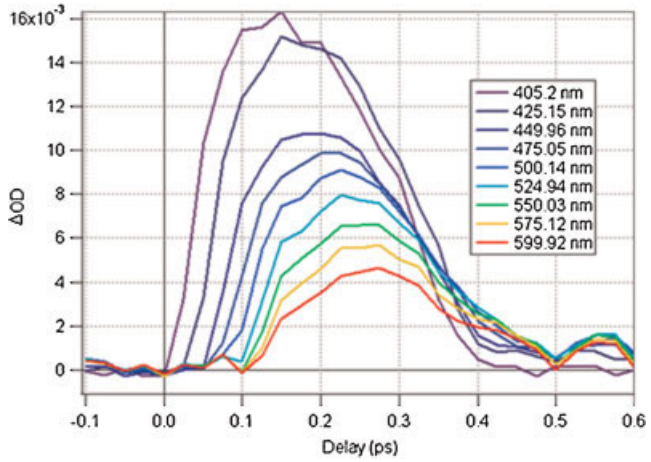

Figure 2. IRF measured in cyclohexane by pump–probe cross correlation ($\lambda_{pump} = 390$ nm).

beam (with pump) and a reference beam (without pump). The transmitted light of the probe and reference beam is recorded on two different channels of a multichannel spectrograph equipped with a CCD camera (Princeton Instrument) and the transient spectra are computed. The transient absorption measurement covers a 400–750 nm spectral range and a 0–5 ns temporal range. The optical density variation ΔOD accuracy is ± 0.001 (before averaging) in the spectral range of the experiments. Sample solution circulates in a flow cell with 1 mm thick CaF_2 windows and is characterized by a 2 mm optical path length. The transient absorption intensity is displayed as a variation of optical density and the spectral data at one time are an average of 4500 spectra. The sample is diluted in cyclohexane at a concentration of 6×10^{-3} mol/L, corresponding to an absorbance of 0.8 at 390 nm in a 2 mm path length cell. All experiments are carried out at 294 ± 2 K.

Salicylidene aniline comes from Sigma-Aldrich, with a purity of 97%, and was used without further purification.

The IRF is assimilated to the pump–probe cross-correlation signal, obtained by measuring the two photon absorption in a thin BK7 microscope clover slip and in a solvent neat solution taking into account cell windows dispersion [6]. Results obtained are shown in Figure 2.

Due to group velocity dispersion, the position of the maximum of the cross correlation peaks is wavelength-dependent and thus the IRF is in general time- and wavelength-dependent. However, as wavelength dispersion is usually corrected by data pretreatment [8], it can be assumed that the IRF is a function of time only [5]. The full-width at half maximum (FWHM) of the IRF is then a reasonable estimate of the time resolution of the experiment (approximately 150 fs in our case), which is assumed to be constant.

3. DECONVOLUTION PROCEDURE

3.1. Convoluted kinetics

Let us denote $C_i(t)$ the undistorded kinetic profile of the pure component i, corresponding to instrumental response that would ideally be instantaneous. In the case of consecutive first-order kinetics, the concentrations are described by linear differential equations and the solution is given by a superposition of N exponential decaying contributions where N is, ideally, the chemical rank, as in Equation (1). In the following, we will restrict our study to the case of consecutive first-order kinetics but it can be extended to second-order consecutive reactions where only one of the reactants do contribute to the signal in the spectral region and to pseudo-first order reactions in general.

$$C_i(t) = \sum_{j=1}^{N} A_j \exp(-k_j t) \tag{1}$$

In Equation (1), the parameter t is the delay time (after photoexcitation) by the coefficients A_j are real values and the parameters k_j are decay rates.

If we consider the convolution of the pure kinetic profiles described by Equation (1) with the effective IRF(t) pulse corresponding to the temporal resolution of the experiment, Equation (2) is obtained.

$$C_i^*(t) = C_i(t) * \mathrm{IRF}(t) = \int_{-\infty}^{\infty} C_i(T-t)\mathrm{IRF}(T)\mathrm{d}T \tag{2}$$

The sign * indicates the operation of convolution and the notation C^* is used thereafter to design convoluted kinetic profiles.

In the following, we consider a Gaussian parametric description of the IRF to be included in the model function, Equation (2). As stated in reference [15], the Gaussian IRF can be well described by setting two parameters, one for the mean of the Gaussian and the other for the FWHM. No wavelength-dependent delay parameter is required here since the spectrokinetic data were corrected for wavelength dispersion before analysis ($t = 0$ centered Gaussian). A single parameter (σ) corresponding to FWHM is thus used. In this case, the IRF can be written as in

$$\begin{aligned} C_i^*(t,\sigma) &= C_t(t) * \mathrm{IRF}(t,\sigma) \\ &= \sum_{j=1}^{N} A_j \left(\exp(-k_j t) * \exp\left(-\frac{t^2}{2\sigma^2}\right)\right) \end{aligned} \tag{3}$$

Rewriting Equation (3) with Equation (2), the analytical expression, Equation (4), is obtained to describe the convolution of the kinetic profiles.

$$C_i^*(t,\sigma) = \sum_{j=1}^{N} A_j \exp\left(\frac{k_j^2\sigma^2}{2} - k_j t\right)\left(1 - \mathrm{erf}\left(\frac{k_j\sigma^2 - t}{\sqrt{2}\sigma}\right)\right) \tag{4}$$

The previous equation is a parameterized description of the IRF included into the model function to convolve the exponential decays. The additional parameter σ may be estimated from the data. Ideally, the IRF should be measured at the excitation wavelength of the experiment. In that case, the width of the IRF may be estimated from the measurement and the parameter σ may be fixed in Equation (4). Otherwise, it should be considered as an additional parameter to be fitted. In Section 5.1, both alternatives will be considered when dealing with simulated data.

3.2. Multivariate curve resolution-alternating least squares (MCR-ALS)

In femtosecond transient absorption experiments, spectrokinetic data **D** ($m \times n$) contain transient spectra collected at m different

delay time points as rows, and time decay traces at n different wavelengths as columns. As the Beer–Lambert law claims, the spectroscopic properties of a mixture of components can usually be written as the superposition of the spectroscopic properties of the individual components weighted by their concentration. So the experimental data **D** can be described assuming a bilinear model as in

$$\mathbf{D} = \mathbf{C}\,\mathbf{S}^{\mathrm{T}} + \mathbf{E} \tag{5}$$

where the concentration matrix **C** ($m \times N$) ideally contains the kinetic profiles of the N pure contributions in the system at m delays and the matrix $\mathbf{S}^{\mathrm{T}}$ ($N \times n$) the corresponding spectral contributions at n wavelengths. The error matrix **E** ($m \times n$) contains the residuals. The observations are usually assumed to contain additive normally distributed noise.

Multivariate curve resolution-alternating least-squares (MCR-ALS) aim at resolving Equation (5). As MCR-ALS has been presented many times in the literature [14], only the main points of the procedure are given thereafter. For the purpose of resolving Equation (5), ALS is used to iteratively fit the **C** and $\mathbf{S}^{\mathrm{T}}$ matrices to the experimental matrix **D**. At each iterative cycle of the optimization, matrices **C** and $\mathbf{S}^{\mathrm{T}}$ are calculated under constraints minimizing the reproduction error **E**. The full MCR-ALS procedure can be summarized in the following steps (holding for situations where concentration profiles are used to start the iterative resolution):

(1) Determination of the chemical rank to the experimental matrix **D** by means of singular value decomposition (SVD) [37].
(2) Construction of initial estimates of concentration profiles **C** using chemometric methods such as evolving factor analysis (EFA) [38] and/or chemical insight.
(3) Given **D** and **C**, least-squares calculation of $\mathbf{S}^{\mathrm{T}} = \mathbf{C}^{+}\,\mathbf{D}$ under suitable constraints (the notation $\mathbf{C}^{+}$ defines the pseudoinverse of **C**).
(4) Given **D** and $\mathbf{S}^{\mathrm{T}}$, least-squares calculation of $\mathbf{C} = \mathbf{D}\,(\mathbf{S}^{\mathrm{T}})^{+}$ under suitable constraints (the notation $(\mathbf{S}^{\mathrm{T}})^{+}$ defines the pseudoinverse of $\mathbf{S}^{\mathrm{T}}$).
(5) Reproduction of **D** using **C** and $\mathbf{S}^{\mathrm{T}}$ calculated in steps (3) and (4). Go back to step (3) until convergence is achieved.

Convergence is achieved when the relative difference in lack of fit between two consecutive iterations goes below a threshold value (often 0.1%) or when a predefined number of iterations are exceeded. The lack of fit gives a measure of the fit quality and is calculated as

$$\text{lack of fit} = \sqrt{\frac{\sum_i \sum_j \left(d_{i,j} - d^{*}_{i,j}\right)^2}{\sum_i \sum_j d^{2}_{i,j}}} \tag{6}$$

Where $d_{i,j}$ and $d^{*}_{i,j}$ denote the elements of **D** and the elements of the reconstructed matrix by the MCR-ALS, respectively.

The introduction of constraints in the ALS procedure is essential to get concentration profiles and spectral contributions with chemical meaning. This also reduces the number of possible solutions for the results (rotational ambiguity). Constraints may be applied to **C** and/or $\mathbf{S}^{\mathrm{T}}$, to all the contributions or to some of them only, globally or to individual sub-matrices when augmented data matrices are considered. Commonly applied constraints in time-resolved spectroscopy are non-negativity and unimodality of the concentration profiles. Normalization is typically applied to the spectra to reduce intensity ambiguities of the results inherent to soft-modeling. In this work, normalization to unit area was set for the spectra.

3.3. Deconvolution of MCR kinetic profiles

The time-dependent concentration profiles obtained from MCR resolution of the spectrokinetic data into pure components are denoted as $\hat{\mathbf{C}}$ in the following ($\hat{\mathbf{S}}$ the corresponding transient spectra, respectively). Deconvolution is performed on the $\hat{\mathbf{C}}$ to recover the decay rate parameters k_j characterizing the true kinetics **C** by fitting $\hat{\mathbf{C}}$ profiles with the model function described in, Equation (4). The additional parameter σ may be either freed or fixed if known from measurement of the IRF (see Section 2) or estimated in another way, thus reducing the number of free parameters. To fit the time-dependent profiles issued from MCR, a classical nonlinear least-square fitting by Newton–Gauss–Levenberg–Marquardt (NGLM) algorithm is used [39,40].

The proposed approach combines mutual benefit of soft-modeling MCR of the process data and of more classical global analysis fitting deconvolution procedure (direct fit of linear combination of convoluted kinetics). In soft-modeling, the process is initially described without using any kinetic model. The resolved concentrations may be considered globally when fitting an external kinetic model, as and when principal component scores are used as input. However, they may also be considered individually, allowing fitting some of them while others are left outside the model to describe non-kinetics contributions. This approach was performed here on single data sets but can be extended to multiset analysis [10,12,14]. All the calculations were made in Matlab 7.1 (The Matworks, Massachusetts, USA). Routines were designed in-house to take into account the deconvolution into the NGLM algorithm and are available on request to the authors. MCR-ALS [41] is freely available on the web at http://www.ub.es/gesq/mcr/mcr.htm

4. DATA SETS

The only way to describe the effect of dealing with convoluted kinetic profiles is to compare with undistorted ones which is, obviously, only possible when dealing with simulated spectrokinetic data. Therefore, situations considering IRF of different FWHM values, and hence different time resolutions of the experiment, are considered. IRF width values from 10 to 200 fs are then covered. The methodology is also applied to the study of femtosecond transient absorption spectroscopy data probing the photochromism of SA in cyclohexane. In that case, the time resolution of the experiment (150 fs) was assessed as explained in Section 2.

4.1. Simulated time-resolved spectroscopic data

The spectrokinetic data sets $\mathbf{D}_1$–$\mathbf{D}_5$ were artificially constructed in general agreement with the previously published results on SA photodynamics (transient absorption spectra and kinetic profiles) [29,30,33]. They contain 400 spectra of 1340 difference optical density (ΔOD) values each. The simulated kinetic model is a sequential four-step reaction $A \xrightarrow{k_1} B \xrightarrow{k_2} C \xrightarrow{k_3} D \xrightarrow{k_4} E$, with rate constants 100, 20, 5 and 0.5 ps^{-1} for k_1, k_2, k_3 and k_4, respectively, i.e. characteristic times 10, 50, 200 fs and 2 ps for τ_1, τ_2, τ_3 and τ_4,

respectively, with $\tau = 1/k$. The kinetic scheme was designed to roughly model the photodynamic properties of SA in solution (see Figure 1). The characteristic time, 50 fs, associated with k_2 would correspond to the ESIPT [7,30,31,33]. The rate constant k_1 typically would describe an ultrafast transition ($\sim$ few femtoseconds) between the ground state and the excited state, which is usually not accessible from classical experimental data. The rate constants k_3 would correspond to the formation of a cis-keto intermediate ($\sim$200 fs) [7,32]. Finally, k_4 would correspond to the relaxation of this intermediate to the trans-keto photochromic form ($\sim$2 ps). The relaxation shown in Figure 1 between the cis-keto intermediate and the ground state gives rise to a minor component (fluorescence quantum yield is about 10^{-4}), which does not absorb in the spectral region of our studies. As we are dealing with difference absorption spectra, it is considered that species *A* do not contribute to the signal in the studied spectral region, meaning that its kinetic profile cannot be recovered from the raw measurement, but, nevertheless, it should be taken into account for setting the kinetic law governing the process [12].

The simulated pure kinetic profiles **C** are convoluted with different IRF, assumed to be normalized centered Gaussian function, giving five kinetic matrices $\mathbf{C}^*_1$ – $\mathbf{C}^*_5$ corresponding to the IRF width $\sigma_1 = 0$ fs, $\sigma_2 = 10$ fs, $\sigma_3 = 50$ fs, $\sigma_4 = 100$ fs and $\sigma_5 = 200$ fs, respectively. The corresponding profiles are represented in Figure 3.

The corresponding simulated spectrokinetic data are obtained considering a matrix **S** containing four difference spectra for contributions *B*, *C*, *D* and *E*, respectively. The matrices $\mathbf{D}_1$–$\mathbf{D}_5$ are calculated according to Equation (5) with an added 2% homoscedastic noise. Figure 4 provides plots of the data sets $\mathbf{D}_1$ and $\mathbf{D}_5$, obtained when an ideal but hypothetical IRF ($\sigma_1 = 0$) is considered on the one hand and a typical situation of transient femtosecond spectroscopy ($\sigma_5 = 200$ fs) is set on the other hand. The time domain considered ranges linearly from 0 to 2.5 ps with a 5 fs step.

4.2. Real femtosecond transient spectroscopy data

Data set **D** was registered using the procedure described in Section 2. It corresponds to transient absorption spectra of SA in cyclohexane at an excitation wavelength of 390 nm represented in Figure 5. The data set is formed from spectra recorded at 1340 wavelength in the range of 400–750 nm. The time domain ranges from 0 to 4.5 ps with a nonlinear time scale (step of 10 fs up to 150 fs, then 25 fs up to 300 fs, 100 fs up to 1.5 ps, 250 fs up to 3 ps and 500 fs to 4.5 ps).

Data were corrected for solvent contributions (strong negative stimulated Raman emission signal peaking at 445 nm) and other possible artifacts that are usually observed during the first picoseconds applying the method proposed in reference [7]. To avoid any distortion on the shape of spectra due to the laser beams, the spectral width of experimental data for MCR analysis is limited to 415–675 nm.

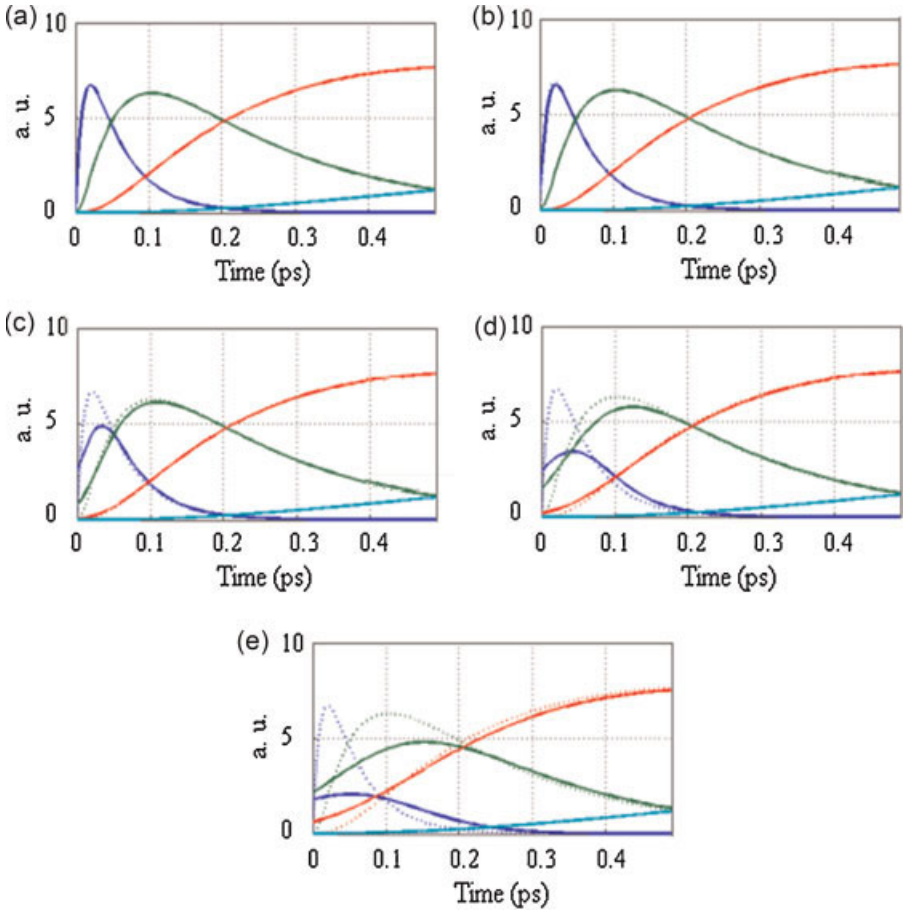

Figure 3. Simulated pure kinetics profiles **C** (dotted lines) and convoluted kinetics profiles $\mathbf{C}^*_1$–$\mathbf{C}^*_5$ (dashed lines) for (a) $\sigma_1 = 0$ fs, (b) $\sigma_2 = 10$ fs, (c) $\sigma_3 = 50$ fs, (d) $\sigma_4 = 100$ fs and (e) $\sigma_5 = 200$ fs, respectively, and for time delay ranging from 0 to 0.5 ps.

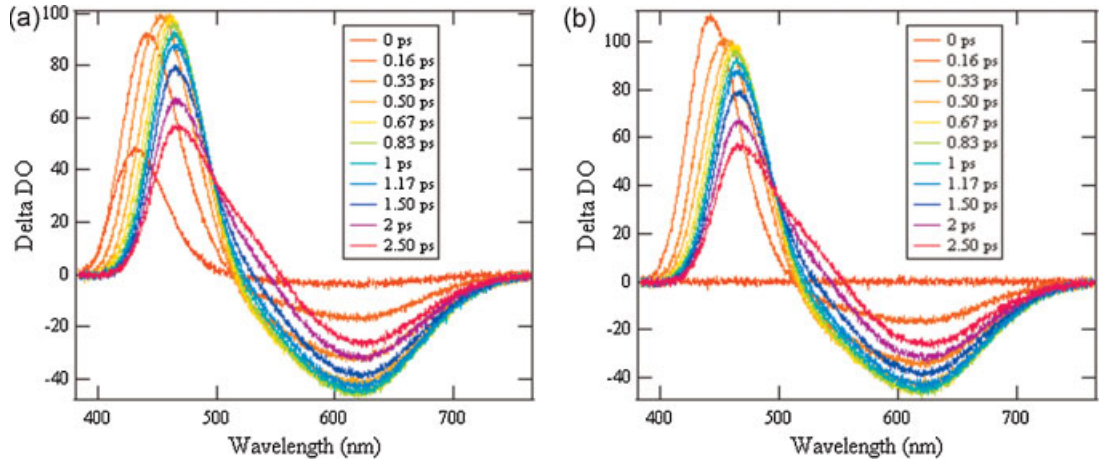

Figure 4. Simulated transient absorption spectra (with a factor 10^{-3}) for (a) the ideal data set $\mathbf{D}_1$ ($\sigma_1 = 0$ fs) and (b) data set $\mathbf{D}_5$ ($\sigma_5 = 200$ fs), and for time ranging from 0 to 2 ps.

5. RESULTS AND DISCUSSION

5.1. Simulated data sets

Transient absorption spectra are difference data (differential spectroscopy is usually used to probe small changes, e.g. when only a small portion of the molecules are absorbed, or in complex environment), the reference being the ground state of the molecule. The examples we deal with show difference data corresponding to first-order kinetic model $A \xrightarrow{k_1} B \xrightarrow{k_2} C \xrightarrow{k_3} D \xrightarrow{k_4} E$, where the signal of the initial contribution A (ground state) is zero in transient absorption spectroscopy. The determination of the chemical rank from the rank analysis must thus be carefully assessed. The singular values of the data sets $\mathbf{D}_1$–$\mathbf{D}_5$ presented in Table I confirm the results expected that the chemical rank of difference data should be the one of direct data minus one [12].

The study of the singular values leads to the following observations: (i) the rank of the data sets indicates four detectable contributions irrespective of the value for the IRF width σ; (ii) when increasing σ values, the singular values are changed in a way that alters the distinction between the minor contributions. This is to be related to the situation depicted previously when σ gets values on the same order, or greater than, as the characteristic time of the considered species (see Figure 1, contributions B and C for instance). More generally, the characteristic times of these contributions become roughly equal to σ due to convolution, i.e. their kinetic profiles have roughly the shape of the Gaussian-IRF (Equations (3), (4)). Nevertheless, in the different situations simulated here, and for reasonable noise levels, it can be concluded that the rank of the data sets $\mathbf{D}_1$–$\mathbf{D}_5$ is still reliably estimated after the convolution of the original kinetics. MCR resolution may thus be attempted on convoluted data without necessarily considering the prior deconvolution of the kinetic traces.

Soft-modeling MCR-ALS was applied to resolve data sets $\mathbf{D}_1$–$\mathbf{D}_5$. In each case, resolution was achieved considering four components. Initial estimates were profiles obtained from EFA. Constraints implemented during the resolution were non-negativity and unimodality of the concentration profiles of the transient contributions. The resolved time-dependent concentration profiles and the corresponding spectra are shown in Figure 6 (only the results obtained for $\mathbf{D}_2$ and $\mathbf{D}_5$ are shown).

When compared to the simulated convoluted profiles, the agreement is good as confirmed by fitting errors (estimated lack of fit are 2.77 and 2.44% for $\mathbf{D}_2$ and $\mathbf{D}_5$, respectively). Nevertheless, as for all soft-modeling techniques, MCR models

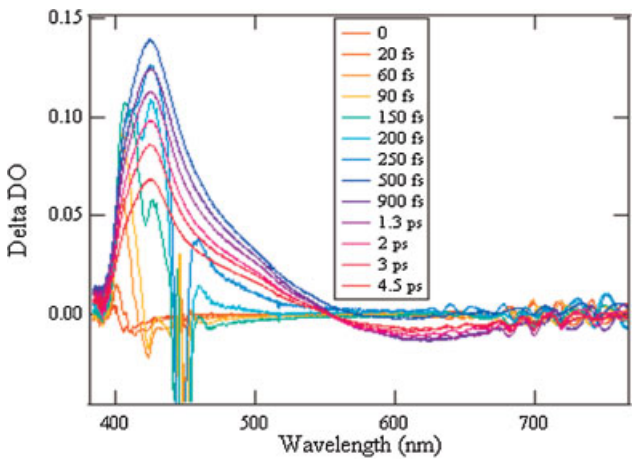

Figure 5. Femtosecond transient absorption spectra of SA in cyclohexane, for time ranging from 0 to 4.5 ps.

Table I. Singular values obtained from SVD (with a factor 10^4) of data matrices $\mathbf{D}_1$–$\mathbf{D}_5$. Only the six first singular values are reported

Data sets	$\mathbf{D}_1$	$\mathbf{D}_2$	$\mathbf{D}_3$	$\mathbf{D}_4$	$\mathbf{D}_5$
Singular values	4.7836	4.7821	4.7747	4.7605	4.7204
1.2408	1.2373	1.2053	1.1559	1.0658	
	0.7741	0.7718	0.7543	0.7264	0.6635
	0.2653	0.2607	0.2187	0.1697	0.1057
	0.0189	0.0191	0.0184	0.0178	0.0169
	0.0188	0.0188	0.0181	0.0177	0.0169
	...	...	...	...	...

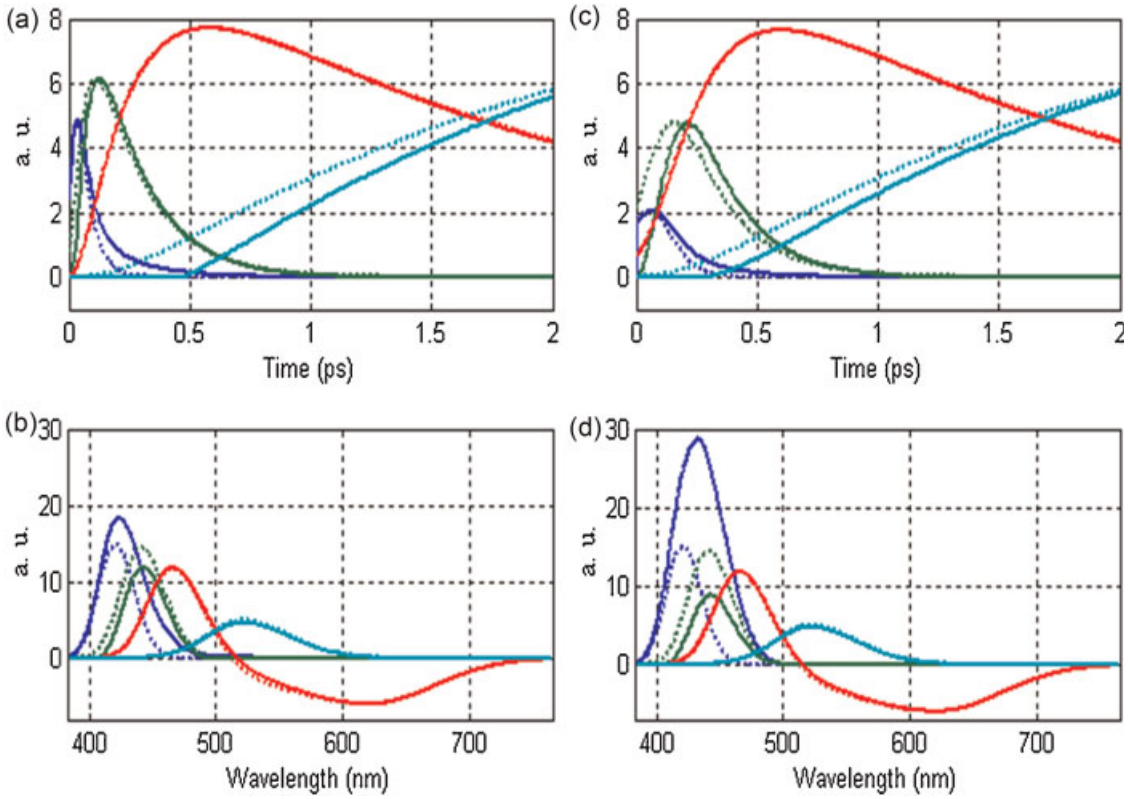

Figure 6. Results of MCR (continuous line) against simulated convoluted profiles (dashed lines) obtained for $\mathbf{D}_2$ ($\sigma_2 = 10$ fs) and for $\mathbf{D}_5$ ($\sigma_5 = 200$ fs) (a) convoluted kinetic profiles $\hat{\mathbf{C}}_2$, (b) transient spectra $\hat{\mathbf{S}}_2$, (c) kinetic profiles $\hat{\mathbf{C}}_5$ and (d) transient spectra $\hat{\mathbf{S}}_5$.

what was measured meaning that the time-dependent concentration profiles extracted from MCR are the convoluted ones. In addition, the signal distortion induced by convolution may propagate to the corresponding $\hat{\mathbf{S}}$ spectra. This is highlighted here for an extreme situation, as in the case of simulated data where the time resolution σ is significantly larger than the shorter characteristic times of the process (see Figure 6c and 6d). It should be added that some differences between the simulated convoluted profiles and those modeled by MCR can already be noticed for the ideal case ($\mathbf{D}_1$). This is due to rotational ambiguity. Indeed, due to the differential nature of time-resolved data, no constraints are applied to the spectra during resolution. As expected, the profiles resolved for the last component are quite significantly affected since no selective time- or spectral window can be found for the latter.

Deconvolution was performed on the estimation of the profiles $\hat{\mathbf{C}}_1$–$\hat{\mathbf{C}}_5$ obtained from MCR. The fitting procedure is based on the model function as described in Equation (4). The results obtained for the characteristic times are provided in Table II.

Two situations are distinguished, depending on whether σ is considered an extra parameter to be fitted, as and when the IRF of the experiment is unknown (Case 1), or a fixed value obtained from the measurement of the IRF for example (Case 2). Considering Case 1 first, the values reported show good overall agreement with the expected characteristic times set for the simulation. Nevertheless, this statement should be qualified for the results obtained for large IRF width values as for data set $\mathbf{D}_5$ ($\sigma_5 = 200$ fs). In this latter case, τ_2 and τ_3 are significantly different from the expected ones, although not erroneous. This was a difficulty expected for increased IRF width, which also illustrate the pertinence of the simulation we are dealing with. Considering Case 2, the same conclusion can be drawn for $\mathbf{D}_1$–$\mathbf{D}_4$: there is no significant difference when compared to the results obtained with free σ parameter. On the contrary, the results obtained for characteristic times τ_2 and τ_3 (52 and 189 fs, respectively) for $\mathbf{D}_5$ are improved when the parameter σ is set to its known value σ_5. It is also observed that fixing the IRF parameter significantly reduces the fitting uncertainties associated to the characteristic times. Nevertheless, rotational ambiguity remains an issue for the resolution of the last species as discussed previously, as it can be noticed from the uncertainty values obtained for $\mathbf{D}_1$–$\mathbf{D}_5$.

5.2. Characterization of the photodynamics of SA

The work on simulated data has shown the possibility to perform reliable kinetic deconvolution on the time-dependent concentration profiles recovered from MCR. The potential of the proposed method to recover the true kinetics has been discussed. The benefit of fixing the IRF width, whenever it can be obtained from experimental procedure, has also been shown. Following the same strategy, the resolution of the femtosecond transient absorption spectra of SA in cyclohexane is performed. Soft-modeling MCR results are shown in Figure 7. Three transient species are resolved. The fitted profiles (continuous lines) are in quite good agreement with the kinetic profiles issued from MCR-ALS (dotted lines) considering the experimental data we are dealing with. A lack of fit of 11.8% was obtained, which was found acceptable. It was also checked that no improvement can be obtained when including different number of components in the resolution. The profiles $\hat{\mathbf{C}}$ and $\hat{\mathbf{S}}$ extracted from MCR analysis

Table II. Characteristic times (in femtoseconds) obtained from the deconvolution of MCR kinetic profiles for the data matrices $\mathbf{D}_1$–$\mathbf{D}_5$ with time resolution $\sigma_1 = 0$ fs, $\sigma_2 = 10$ fs, $\sigma_3 = 50$ fs, $\sigma_4 = 100$ fs and $\sigma_5 = 200$ fs, respectively

	Parameter	Target values	$\mathbf{D}_1$ $\sigma_1 = 0$ fs	$\mathbf{D}_2$ $\sigma_2 = 10$ fs	$\mathbf{D}_3$ $\sigma_3 = 50$ fs	$\mathbf{D}_4$ $\sigma_4 = 100$ fs	$\mathbf{D}_5$ $\sigma_5 = 200$ fs
Case 1 (free σ)	σ	—	11.95 (± 0.72)	9.65 (± 0.77)	55.08 (± 3.83)	100.42 (± 3.12)	141.58 (± 64.05)
	τ_1	10	9.27 (± 0.15)	9.77 (± 0.21)	11.44 (± 1.11)	10.74 (± 1.46)	11.17 (± 5.35)
	τ_2	50	49.53 (± 0.28)	49.30 (± 0.15)	49.27 (± 0.99)	50.31 (± 2.98)	71.09 (± 4.41)
	τ_3	200	191.52 (± 0.43)	195.85 (± 8.90)	190.48 (± 20.47)	201.81 (± 9.61)	169.42 (± 14.65)
	τ_4	2000	1 976.80 (± 4.48)	1 993.00 (± 11.10)	1 950.10 (± 12.10)	1 904.20 (± 7.77)	1 961.80 (± 13.10)
Case 2 (fixed σ^a)	τ_1	10	10.23 (± 0.07)	9.61 (± 0,12)	11.31 (± 0.89)	12.55 (± 4.29)	10.25 (± 0.13)
	τ_2	50	49,27 (± 0.17)	49.52 (± 0.28)	49.82 (± 0.41)	49.01 (± 1.54)	52.33 (± 1.68)
	τ_3	200	197.67 (± 0.82)	197.52 (± 1.22)	186.67 (± 0.76)	196.98 (± 10.06)	189.02 (± 4.10)
	τ_4	2000	1 942.6 (± 9.56)	2 037.7 (± 37.80)	1 959.90 (± 30.60)	1 959.90 (± 21.56)	1 947.4 (± 6.61)

[a] The value of σ is fixed to σ_1–σ_5 for $\mathbf{D}_1$–$\mathbf{D}_5$, respectively.

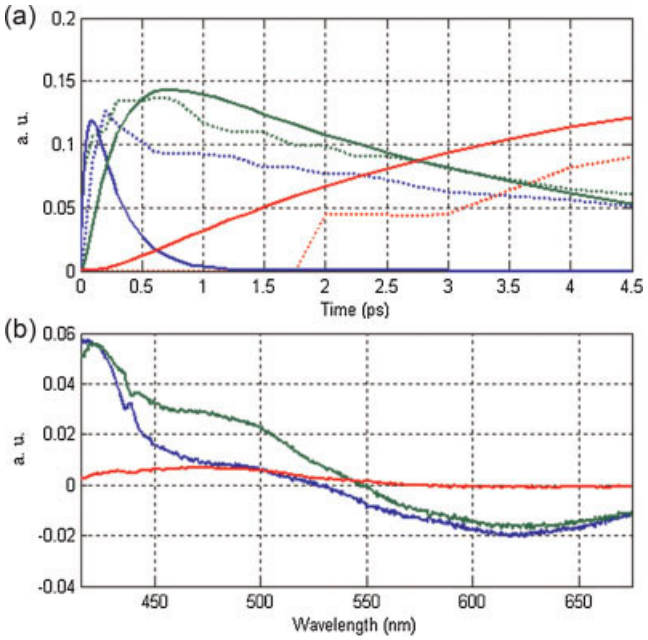

Figure 7. Profiles extracted from MCR (dotted lines) compared with convoluted kinetic profiles fitted (continuous lines) for femtosecond transient absorption experiment of SA in cyclohexane (a) time-dependent concentration profiles, and (b) transient spectra.

are also found in quite good agreement with results obtained previously for this class of molecules in different solvents [7,31,32].

Deconvolution was performed on the kinetic profiles $\hat{\mathbf{C}}$ obtained from MCR. A temporal resolution of 150 fs was considered in the fitting procedure. This value is distinctive of our set-up and experimental conditions. As explained earlier, a first-order kinetic model can be assumed to describe the photodynamic properties of SA. The values for the rate constants obtained are 22 (±0.16), 4 (±0.03) and 0.28 (±0.67.10^{-2}) ps^{-1}, which correspond to 45 fs, 241 fs and 3.53 ps characteristic times for deconvoluted kinetic profiles, respectively (see also Figure 1). The characteristic time 45 fs corresponds to the growing of the first species. The associated spectrum characterizes the cis-keto* excited state issued from the ESIPT, i.e. the species *C* in Figure 1 [7,30,31,33]. Indeed, it presents a negative part for wavelengths above 550 nm, corresponding to the stimulated emission of cis-keto*. The species *D* obtained after resolution and deconvolution have similar spectra to that created by the ESIPT (species *C*). The positive part of the spectrum is attributed to the transient absorption of S_1 fluorescent cis-keto*. The spectral width (around 420 nm) is narrower than species *C* and slightly shifted to the red part, which is a characteristic of vibrational relaxation and slightly different geometry. Species *D* relaxes in few picoseconds to species *E* which is the trans-keto form. Then the spectra associated with species *C* is assimilated to the hot S_1 cis-keto* state, appearing as supposed in less than 50 fs and relaxing to species *D*, which is assigned to the S_1 cold fluorescent cis-keto* state, in a few hundreds of femtosecond. The time decays recovered here show good agreement with those obtained recently by Rodriguez-Cordoba *et al.* in a different solvent [29]. The slight difference of geometry for the species created after the ESIPT and the S_1 fluorescent cis-keto* state was also predicted by Ortiz-Sanchez *et al.* [30].

6. CONCLUDING REMARKS

For processes with characteristic times shorter than the time resolution of the experiment, the principle of deconvolution of the kinetic profiles obtained from MCR has been demonstrated for consecutive first-order kinetic process. The method can readily be extended to process where the kinetic profiles are described by a sum of exponentials with tailored fitting functions. Benefits of the proposed approach are those of soft-modeling MCR methods: (i) no explicit model is required for component resolution making data exploration possible, (ii) external kinetic fitting (and deconvolution) can be performed on the profiles and (iii) as time-dependent profiles are corresponding to pure components (ideally), they may be considered globally or individually in further data treatment. However, some limitations are pointed out regarding (i) the nature of the investigated process (described as a sum of exponential functions) and (ii) rotational ambiguity of soft-modeling resolutions. Special attention should be paid to this latter point when dealing with difference data as non-negativity constraint does not hold for the spectra. For this reason, the integration of convoluted kinetic models in hybrid hard- and soft-MCR procedure [17] to resolve ultrafast spectrokinetic data is currently under investigation.

Acknowledgements

The authors are grateful to Professor A. de Juan from the department of Analytical Chemistry of the University of Barcelona for fruitful discussion. N. Mouton acknowledges a PhD scholarship from the Ministère de l'enseignement supérieur et de la recherche.

REFERENCES

1. Norrish RGW, Porter G. Chemical reactions produced by very high light intensities. *Nature* 1949; **164**: 658.
2. de Schryver FC, de Feyter S, Schweitzer G. *Femtochemistry*. VCH: New York, 2001.
3. Diels JC, Rudolph W. *Ultrashort Laser Pulse Phenomena. Fundamentals, Techniques and Application on a Femtosecond Time Scale*. Academic Press: London, 1996.
4. Tamai N, Miyasaka H. Ultrafast Dynamics of Photochromic Systems. *Chem. Rev.* 2000; **100**: 1875.
5. Lorenc M, Ziolek M, Naskrecki R, Karolczak J, Kubicki J, Maciejewski A. Artifacts in femtosecond transient absorption spectroscopy. *Appl. Phys. B-Laser. Opt.* 2002; **74**: 19.
6. Ziolek M, Lorenc M, Naskrecki R. Determination of the temporal response function in femtosecond pump-probe systems. *Appl. Phys. B-Laser. Opt.* 2001; **72**: 843.
7. Ruckebusch C, Sliwa M, Rehault J, Naumov P, Huvenne JP, Buntinx G. Hybrid hard- and soft-modelling applied to analyze ultrafast processes by femtosecond transient absorption spectroscopy: Study of the photochromism of salicylidene anilines. *Anal. Chim. Acta* 2009; **642**: 228.
8. Nakayama T, Amijima Y, Ibuki K, Hamanoue K. Construction of a subpicosecond double-beam laser photolysis system utilizing a femtosecond Ti: sapphire oscillator and three Ti: sapphire amplifiers (a regenerative amplifier and two double passed linear amplifiers), and measurements of the transient absorption spectra by a pump-probe method. *Rev. Sci. Instrum.* 1997; **68**: 4364.
9. Aloise S, Ruckebusch C, Blanchet L, Rehault J, Buntinx G, Huvenne JP. The benzophenone S-1(n,pi*) → T-1(n,pi*) states intersystem crossing reinvestigated by ultrafast absorption spectroscopy and multivariate curve resolution. *J. Phys. Chem. A* 2008; **112**: 224.
10. Ruckebusch C, Aloise S, Blanchet L, Huvenne JP, Buntinx G. Reliable multivariate curve resolution of femtosecond transient absorption spectra. *Chemom. Intell. Lab. Syst.* 2008; **91**: 17.
11. von Frese J, Kovalenko SA, Ernsting NP. Interactive curve resolution by using latent projections in polar coordinates. *J. Chemom.* 2007; **21**: 2.
12. Blanchet L, Ruckebusch C, Huvenne JP, de Juan A. Hybrid hard- and soft-modeling applied to difference spectra. *Chemom. Intell. Lab. Syst.* 2007; **89**: 26.
13. Tauler R. Multivariate curve resolution applied to second order data. *Chemom. Intell. Lab. Syst.* 1995; **30**: 133.
14. de Juan A, Tauler R. Multivariate curve resolution (MCR) from 2000: progress in concepts and applications. *Crit. Rev. Anal. Chem.* 2006; **36**: 163.
15. van Stokkum IHM, Larsen DS, van Grondelle R, Global and target analysis of time-resolved spectra. *Biochim. Biophys. Acta-Bioenerg.* 2004; **1657**: 82.
16. Amigo JM, de Juan A, Coello J, Maspoch S. A mixed hard- and soft-modelling approach to study and monitor enzymatic systems in biological fluids. *Anal. Chim. Acta* 2006; **567**: 245.
17. de Juan A, Maeder M, Martinez M, Tauler R. Combining hard- and soft-modelling to solve kinetic problems. *Chemom. Intell. Lab. Syst.* 2000; **54**: 123.
18. Blanchet L, Rehault J, Ruckebusch C, Huvenne JP, Tauler R, de Juan A. Chemometrics description of measurement error structure: study of an ultrafast absorption spectroscopy experiment. *Anal. Chim. Acta* 2009; **642**: 19.
19. Banyasz A, Matyus E, Keszei E. Deconvolution of ultrafast kinetic data with inverse filtering. *Radiat. Phys. Chem.* 2005; **72**: 235.
20. McKinnon AE, Szabo AG, Miller DR. Deconvolution of photoluminescence data. *J. Phys. Chem.* 1977; **81**: 1564.
21. Banyasz A, Keszei E. Model-free deconvolution of femtosecond kinetic data. *J. Phys. Chem. A* 2006; **110**: 6192.
22. Keszei E. Efficient model-free deconvolution of measured femtosecond kinetic data using a genetic algorithm. *J. Chemom.* 2009; **23**: 188.
23. Bouas-Laurent H, Durr H. Organic photochromism. *Pure Appl. Chem.* 2001; **73**: 639.
24. Dürr H, Bouas-Laurent H. *Photochromism: Molecules and Systems*. Elsevier: Amsterdam, Netherlands, 1990.
25. Raymo FM, Alvarado RJ, Giordani S, Cejas MA. Memory effects based on intermolecular photoinduced proton transfer. *J. Am. Chem. Soc.* 2003; **125**: 2361.
26. Irie M. Photochromism: memories and switches - Special issue. *Chem. Rev.* 2000; **100**: 1683.
27. Amimoto K, Kawato T. Photochromism of organic compounds in the crystal state. *J. Photochem. Photobiol. C* 2005; **6**: 207.
28. Hadjoudis E, Mavridis IM. Photochromism and thermochromism of Schiff bases in the solid state: structural aspects. *Chem. Soc. Rev.* 2004; **33**: 579.
29. Rodriguez-Cordoba W, Zugazagoitia JS, Collado-Fregoso E, Peon J. Excited state intramolecular proton transfer in schiff bases. Decay of the locally excited enol state observed by femtosecond resolved fluorescence. *J. Phys. Chem. A* 2007; **111**: 6241.
30. Ortiz-Sanchez JM, Gelabert R, Moreno M, Lluch JM. Electronic-structure and quantum dynamical study of the photochromism of the aromatic Schiff base salicylideneaniline. *J. Chem. Phys.* 2008; **129**: 11.
31. Ziolek M, Kubicki J, Maciejewski A, Naskrecki R, Grabowska A. An ultrafast excited state intramolecular proton transfer (ESPIT) and photochromism of salicylideneaniline (SA) and its "double" analogue salicylaldehyde azine (SAA). A controversial case. *Phys. Chem. Chem. Phys.* 2004; **6**: 4682.
32. Mitra S, Tamai N. Dynamics of photochromism in salicylideneaniline: A femtosecond spectroscopic study. *Phys. Chem. Chem. Phys.* 2003; **5**: 4647.
33. Sliwa M, Mouton N, Ruckebusch C, Métivier R, Nakatani K, Aloise S, Poizat O, Buntinx G, Masuhara H, Asahi T. Comparative investigation of ultrafast photoinduced processes in salicylidene-aminopyridine in solution and solid-state. *J. Phys. Chem. C* 2009; **113**(1): 1959.
34. Okabe C, Nakabayashi T, Inokuchi Y, Nishi N, Sekiya H. Ultrafast excited-state dynamics in photochromic N-salicylideneaniline studied by femtosecond time-resolved REMPI spectroscopy. *J. Chem. Phys.* 2004; **121**: 9436.

35. Buntinx G, Naskrecki R, Poizat O. Subpicosecond transient absorption analysis of the photophysics of 2,2′-bipyridine and 4,4′-bipyridine in solution. *J. Phys. Chem.* 1996; **100**: 19380.
36. Moine B, Rehault J, Aloise S, Micheau JC, Moustrou C, Samat A, Poizat O, Buntinx G. Transient absorption studies of the photochromic behavior of 3H-naphtho[2,1-b]pyrans linked to thiophene oligomers via an acetylenic junction. *J. Phys. Chem. A* 2008; **112**: 4719.
37. Golub GH, Loan CFV. *Matrix Computation*. The John Hopkins University Press: London, 1989.
38. Maeder M. Evolving factor- analysis for the resolution of overlapping chromatographic peaks. *Anal. Chem.* 1987; **59**: 527.
39. Levenberg KQ. A method for the solution of certain non-linear problems in Least-squares. *Appl. Math.* 1949; **2**: 164.
40. Marquardt DW. An algorithm for least-squares estimation of non-linear parameters. *J. Soc. Ind. Appl. Math.* 1963; **11**: 431.
41. Jaumot J, Gargallo R, de Juan A, Tauler R. A graphical user-friendly interface for MCR-ALS: A new tool for multivariate curve resolution in MATLAB. *Chemom. Intell. Lab. Syst.* 2005; **76**: 101.